Global Comparisons of Regional Life Cycle Properties and Motion of Multiday Convective Systems: Tropical and Midlatitude Land and Ocean

BRIAN VANT-HULL

NOAA–Cooperative Remote Sensing and Technology Institute, City College of the City University of New York, New York, New York

WILLIAM ROSSOW AND CINDY PEARL

Remote Sensing of Climate Group, NOAA–Cooperative Remote Sensing and Technology Center, City College of the City University of New York, New York, New York

(Manuscript received 7 October 2015, in final form 9 May 2016)

ABSTRACT

Tracking of convective cloud systems (cloud-top temperature <245 K) in geosynchronous satellite images at 3-h intervals is used to determine life cycle statistics of convective systems in four regimes: tropical land and ocean and midlatitude land and ocean, including seasonal comparisons. The ISCCP tracking dataset covers the period 1984–2006. Only systems with lifetimes greater than or equal to 1 day that were moving predominantly eastward or westward are considered, with splits and merges combined into larger extended convective systems. The life cycle variables are lifetime (duration), maximum area, and minimum cloud-top temperature. These are compared to each other and to the speed of longitudinal motion. Distributions and relationships between the life cycle variables are similar to previous studies based on single-day lifetimes, but the current study is globally extensive (all longitudes at lower and middle latitudes) and multidecadal, which allows extension of such results to rarer, larger, and longer-lived convective systems than previous work. Velocity distributions were monomodal with tails skewed in the direction of the zonal mean wind, being almost purely eastward in the midlatitudes but nearly symmetric in both directions with a small westward bias in the tropics. Representative life cycles for each geographical region are formed by averaging together systems with similar lifetimes. These composite life cycles show that, except for the first and last days, the daily evolution of most system variables exhibits little variation during the average multiday convective life cycle, although the cloud area goes through one cycle of expansion and contraction in a lifetime.

1. Introduction

Globally extensive studies of cloud properties became feasible with the satellite era starting with the advent of polar-orbiting and geosynchronous satellites in the mid-1970s. In the following decades a number of global studies were performed: mesoscale convective complexes (MCCs) were described (Maddox 1980), cloud types classified and their motion vectors catalogued (Lau and Crane 1995; Joyce et al. 2004), cloud geometry analyzed (Cahalan and Joseph 1989; Wood and Field 2011), overall properties and diurnal cycle of convective clouds analyzed (Gray and Jacobson 1977; Machado and Rossow 1993; Yang and Slingo 2001), and microphysical properties catalogued (Han et al. 2002). The International Satellite Cloud Climatology Program (ISCCP) was established in 1982 to globally catalogue cloud radiative properties (Rossow and Schiffer 1991, 1999). A "weather state" classification based on clustering of ISCCP cloud properties on a 2.5° latitude–longitude grid provides a simple observational proxy for a suite of interrelated weather variables (Rossow et al. 2005; Jakob and Schumacher 2008; Oreopoulos and Rossow 2011; Tselioudis et al. 2013; Rossow et al. 2016).

Notably absent are global studies of cloud life cycles. A number of regional studies have been done with time scales ranging from months to several years, but such work would benefit from a global dataset for comparison. McAnelly and Cotton (1989) tracked 122 storm systems across North America, finding regional variations in the

Corresponding author address: Brian Vant-Hull, NOAA-CREST, Steinman Hall, City College of New York, New York, NY 10031.
E-mail: brianvh@ce.ccny.cuny.edu

DOI: 10.1175/JCLI-D-15-0698.1

time of maximum rainfall during the typical 10-h life cycle. Machado et al. (1998) studied two years of MCS life cycle statistics over the Western Hemisphere for North and South America viewed by GOES-East, for typical lifetimes less than 1 day. They found a nearly linear increase in maximum radius and a decrease in minimum temperature over life cycles up to 27 h. Further work over two months over Amazonia (Machado and Laurent 2004) found that the logarithm of the area evolved parabolically with time, and initial area expansion was a good predictor not just of the maximum radius, but also of rainfall. Futyan and Del Genio (2007) found that four months of composited life cycle plots over Africa were skewed in comparison to those Machado found over the Americas, with systems changing to warmer cloud tops as they passed from land to sea. An examination of four months of the geographical patterns in the convective life cycle over the western Pacific led Chen and Houze (1997) to propose that previous passage of convective systems affected the local environment to suppress convection for the next day. In one of the few investigations of multiday convective systems, a 2-yr study over the Indian Ocean found that the correlation between maximum radius and lifetime increased for colder cloud detection thresholds, and warm convective clouds were found to travel faster than deep convective clouds (Gambheer and Bhat 2000). Pope et al. (2008) tracked clouds over northern Australia and the surrounding oceans, finding the same quasi-linear relationships between lifetime and maximum radius reported in Machado et al. (1998) and Machado and Laurent (2004), but found that the relationship weakened as cloud merges were included and nearly disappeared as the lifetimes extended beyond a single day.

Considerable interest has been generated by the mystery behind the propagation of convective systems seen in the Madden–Julian oscillation (Madden and Julian 1972; Zhang 2013), which is a convective anomaly typically initiated in the Indian Ocean that propagates eastward along the equator, against the zonal average flow. Close inspection reveals that small convective structures within the larger envelope are moving westward (the zonal average wind direction) even while the larger system propagates eastward (Nakazawa 1988; Lau et al. 1991; Mapes and Houze 1993). There are many theories behind the anomalous propagation [see reviews by Matthews (2000) and Zhang (2005) or compare more recent investigations by Seo and Kim (2003) and Sobel and Maloney (2013)]. The MJO is considered a global-scale wave that does not fit the standard equatorial convectively coupled wave categories (Wheeler and Kiladis 1999; Chang 1976). It is most frequently defined and studied using coarse scale approaches such as outgoing longwave radiation (OLR) or upper-level wind divergence at resolutions of 1° or more to filter out cloud-scale "noise" from the global-scale signal (Rui and Wang 1990; Madden 1986; Masunaga 2007; Wheeler and Hendon 2004). Other better-understood convectively coupled waves are studied using the same methods (Wheeler and Kiladis 1999), often exhibiting the structure of cloud and wave propagation at different velocities. Although we should not expect to capture the full wave properties in our "bottom up" approach, it is of interest to see if the cloud system properties in some way reflect those of the large-scale waves, providing a view of interactions between the two scales.

Cloud tracking relies on matching cloud objects between images. There is a range of approaches to this step (Machado et al. 1998), from simple overlap to spatial correlation. EUMETSAT's rapidly developing thunderstorm algorithm (Morel et al. 2002) advects cells before looking for an overlap; if no overlap is available it performs a local search to find a cell with the closest spatial correlation. The warning decision support system–integrated information (WDS-II) algorithm (Lakshmanan et al. 2007) used by the National Severe Storm Forecast Center skips the overlap step and relies completely on a spatial correlation search. The ISCCP tracking algorithm upon which this paper is based uses the simple overlap method, justified if the expected cloud speeds are smaller than the ratio of the size of the cloud cells divided by the time step between images (Machado et al. 1998).

The current work appears to be the first global study of the life cycle statistics of multiday convective systems. After the introduction of the experimental design and dataset, a number of statistical analyses are performed, each with brief discussion. These are then compared to address the question of propagation velocities, followed by a summary of global properties captured by this analysis.

2. Overview of the analysis

The goal of this work is to examine differences between long-lived convective systems (lifetimes >1 day) categorized by latitude zone, over land or ocean, and by direction of motion (eastward or westward) with comparison to the direction of annual average zonal winds. Seasonality is included. To this end convective systems are tracked that fall within 20°S and 20°N (tropics) and between 30° and 55° latitude in both Northern and Southern Hemispheres (midlatitudes) as shown in Fig. 1. Further division into land and sea results in four geographical zones. After a brief survey of the seasonality of these multiday systems, the study is confined to either annual averages in each latitude zone, or summer and

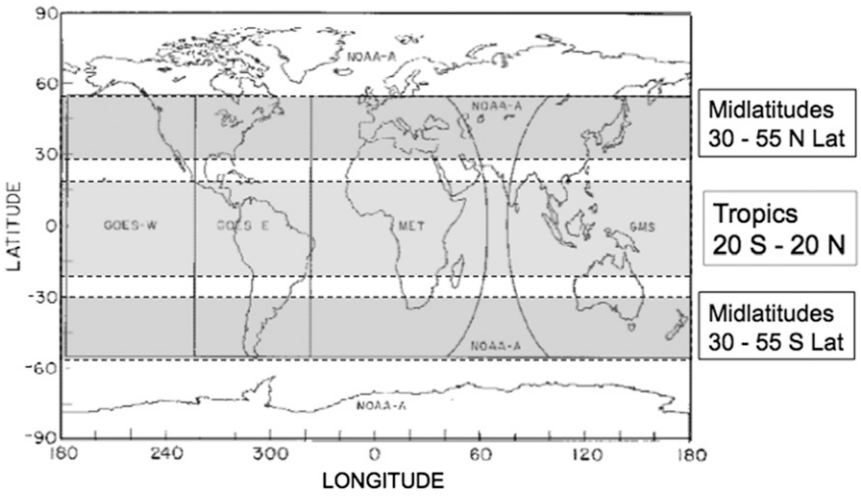

FIG. 1. Satellite domains and latitude zones. The ISCCP domains in solid lines loosely indicate each satellite's field of view, but with overlap regions assigned to single satellites (see Fig. 3 for the full fields of view). Data from the north and south midlatitude zones are combined for most analysis in this study. The tropical and midlatitude zones are further subdivided into land and sea, resulting in four geographical zones total.

winter for which the Northern and Southern Hemispheres are combined according to the appropriate season (JJA or DJF) and the tropics are classified by the Northern Hemisphere summer or winter seasons.

The majority of analysis presented here concerns convective systems that are moving eastward or westward, so that systems that have a meridional velocity component greater than 3° latitude day^{-1} ($\sim 4\,m\,s^{-1}$) are removed from the dataset. Note that this tends to eliminate systems moving meridionally along coastlines due to seasonal land–sea contrast effects. For some of the analysis that follows, zonal velocities less than 3° latitude day^{-1} are also removed, segmenting the convective systems into those that are clearly moving eastward or westward. This speed threshold in both meridional and zonal directions was chosen to capture systems that resemble the MJO (Rui and Wang 1990; Chang 1977; Nakazawa 1988); in combination with the lower limit on lifetime it also eliminates smaller Rossby wave–induced motion. The northward monsoon coupled interseasonal oscillation (ISO) falls within the meridional limits but would be eliminated if zonal lower limits were applied (Yasunari 1979; Jiang et al. 2004). Monsoonal convergence from east and west may remain (Pope et al. 2008). The velocity filters remove from 8% (midlatitude oceans) to 19% (tropical oceans) of multiday cloud systems from the total dataset, with very similar amounts of the total cloud area removed.

Variables descriptive of convective systems such as cloud-top temperature, area, lifetime, and convective fraction are compared to each other and plotted as life cycle averages. Life cycle extremes (maximum equivalent radius, minimum average cloud-top temperature, etc.) are often used for comparison. Since this is the first global study of its kind, the goal is descriptive, not analytic. It is a catalog of properties of multiday convective systems classified by latitude zone and direction of motion.

3. Dataset

This work relies exclusively on ISCCP's deep convection tracking (CT) database (available online at http://crest.ccny.cuny.edu/rscg/products.html), in which clouds are tracked in successive images by the method of overlap (Machado et al. 1998). It is based on the cloud detection scheme of the ISCCP pixel level (DX) data for which cloudy pixels are distinguished from clear sky due to variability in space and time (Rossow and Gardner 1993a, b; Rossow and Schiffer 1999; Rossow et al. 1996). The use of blackbody infrared temperature with an upper limit of 245 K eliminates some thin cirrus. The DX data are composed of satellite pixels sampled at 30-km intervals every 3 h. Given this time step and a typical geostrophic cloud speed of approximately 30 km h^{-1}, the overlap method precludes tracking of cloud clusters smaller than 90 km in diameter.

In cloud tracking literature it is common to refer to successive image pixel clusters in the same cloud cell life cycle as "mother and daughter" or "father and son." In this context the set of image clusters that make up an entire life cycle (or observed portion thereof) might be referred to as a "family." Families may split and merge, and the whole set of joined families may thus be termed a "tribe"—comprising the entire set of cloudy pixels that are contiguous across both time and space. The original

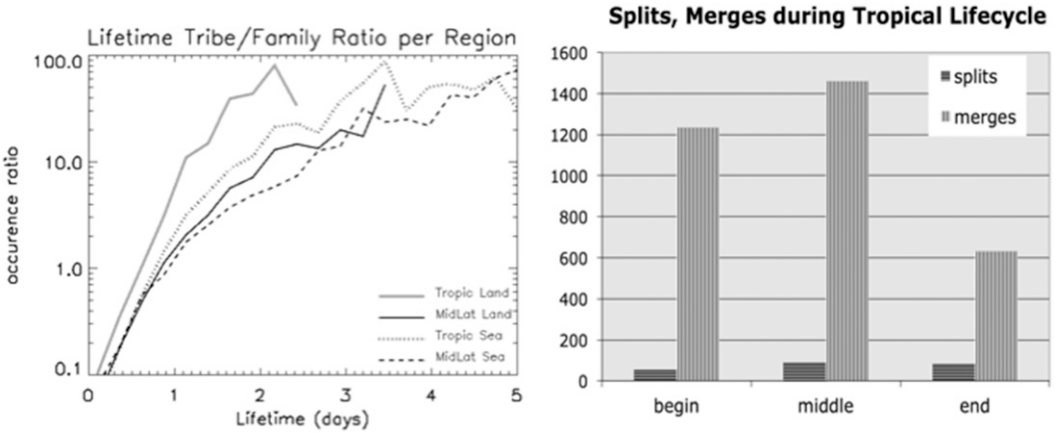

FIG. 2. (left) Ratio of tribes to lone families as a function of lifetime. (right) Number of splits and merges during each equal section of the convective lifetime.

dataset does not group families into tribes, so for this work grouping was done by identifying coincident cells from different families. Splits were also added via the method of overlap because the original dataset only followed the largest overlap cell. Some convective systems do not experience merges or splits between cloud clusters and are hereafter referred to as lone families, whereas those that do have been referred to as tribes. As this is a modification of the dataset currently available online, a brief examination of the nature of splits and merges is appropriate here.

The left panel of Fig. 2 shows the annual average ratio of tribes to lone families for the four geographic regions (tropical land and ocean; midlatitude land and ocean). For lifetimes under 1 day, lone families predominate, but the tribe component increases with lifetime until systems that last 1 day have nearly equal numbers of tribes and lone families. Above 1-day lifetimes tribes increasingly predominate, as longer-lived systems have more chances to meet other systems. For all lifetimes the tropical lands are more likely to exhibit the more complex tribal behavior, likely due to larger radii (see Fig. 5 and Table 1).

In right panel of Fig. 2, the life cycle is divided into thirds (beginning, middle, and end), with all tropical westward-moving systems added together (other regions and directions of motions are similar). The average number of splits and merges is shown, and it is evident that splits are outnumbered almost 20 times by merges. There are predictably fewer splits in the beginning and fewer merges at the end of the life cycle. These results are for multiday systems, and need not agree with the 3:1 ratio seen in single-day studies (Machado et al. 1998; Carvalho and Jones 2001).

This work draws from the entire global ISSCCP CT dataset from 1984 to 2006. Four geosynchronous satellites are used to observe Earth at any given time, and their areas of coverage are referred to as Japanese Geostationary Meteorological Satellite (GMS), GOES-West (GOW), GOES-East (GOE), and EUMETSAT Meteorological Satellite (MET) (see Fig. 1). Gaps between these satellites are filled in by polar-orbiting satellites in most ISCCP data, but not for the CT dataset due to low repeat frequency. In the current incarnation of CT, the cloud families do not continue from one satellite region to another, so the regions will have lifetime bias imposed by the field of view boundaries. Data are stored by satellite and month. Where the satellites overlap, families that cross into the overlap area are stored with the initiating satellite region. Families that cross monthly divisions are likewise stored with the initiating month dataset.

As the dataset is intended to track deep convection, a convective system (CS) is first identified as contiguous cloudy pixels with cloud-top temperatures below 245 K. Within these systems may be convective cores (CC) identified by cloud-top temperatures below 220 K (Fu et al. 1990). If no CC are found, the object is excluded from the dataset. Such objects are often called mesoscale convective systems (MCSs), which would include squall lines, but the dataset also includes hurricanes and typhoons. In the literature MCSs are sometimes referred to as ''organized convection'' in contrast to shorter-lived ''disorganized convection'' (Moncrieff 2004; Tromeur and Rossow 2010). CS characteristics used in this study include area, average cloud-top temperature, number of CC within a CS, and fraction of CS area covered by CC. Equivalent radius is calculated based on a circle with the same area of a given cloud (or total set of clouds if a tribe). Speed and direction are calculated from location and temporal information as described in the next paragraph. Other information included in the dataset for both CS and CC but not used for this study includes

geometry and orientations of the equivalent ellipse, standard deviation and gradient of the cloud-top temperature, and average optical thickness.

Even when constrained to long-lived systems moving mainly eastward or westward, splits and merges between families in a cloud tribe lead to highly complex and tangled paths. Different segments of a tribe existing at the same time may grow or dissipate at varying rates, leading to a highly variable geometry with a rapidly and discontinuously shifting centroid. Tribe velocity has no one obvious definition in this situation, so the simplest approach is adopted: average motions are calculated from the centroids of the first and last appearing cloud cells in a tribe. It should be noted that these temporal end points often do not represent the full geographical extent of the tribe, although these ambiguities are only significant for stationary or slow-moving systems. All analysis done in this paper has also been done with the subset of simple cloud families (no splits or merges) with similar results; we have opted to include the messier cloud tribes for larger datasets to improve statistics.

Cloud-top temperature can be represented several ways: the temperature of the pixel with minimum temperature, the average temperature of all pixels in a cloud, etc. In life cycle studies it is useful to have a single value to represent the extremes, such as maximum radius or coldest temperature. To avoid having a single pixel represent the entire system, the phrase "minimum average temperature" will be used to represent the spatial average temperature (over all pixels in the cloud or set of clouds in the tribe) at the time in the life cycle when it is lowest. The convective core fraction (fraction of pixels colder than 220 K) will be used to represent the coldest points in a cloud.

The zonal annually averaged winds are westward in the tropics and eastward in the midlatitudes. It is of interest to compare systems that move with or opposite to these average flows, with the understanding that the tropics have strong seasonal monsoons that at times overshadow the zonal mean flow. The next section provides a survey of these systems, concentrating on those with lifetimes greater than 1 day. Individual variable surveys are followed by relationships between variables. Each figure is accompanied by the method used to produce it and a brief discussion of how it fits into our current physical understanding.

4. Results

a. Monthly and regional variation in number of MCS tracks

In Fig. 3 the globe is divided into 10° latitude zones from 50°S to 50°N, and the number of zonally moving multiday convective systems (as described in the analysis overview) is tabulated over the two decades period and normalized by area (number of occurrences per million square kilometers of the region). The systems are classified by land or ocean; eastward or westward moving.

The two most obvious features of Fig. 3 are the similarity between land and ocean, and the confinement of westward motion to the tropics. Seasonality shown by the horizontal axis has tropical eastward-moving MCS at a global minimum in July and (although not shown in these diagrams) at a maximum geographically in the western Pacific. Although this tendency is consistent with the observed seasonality of the Madden–Julian oscillation (Madden and Julian 1972; Wang and Rui 1990), the smaller scale of the clouds tracked with their tendency to move opposite to MJO propagation (Nakazawa 1988) suggests we must look elsewhere for explanation, and we leave it for future study. We assume that frontal systems are included, as no constraints on cloud geometry has been imposed.

A clearer view of the seasonality is obtained by binning the data into tropics and midlatitudes (see Fig. 1), land and ocean, and divided into eastward and westward motions: this system is followed for the remainder of the paper.

The minimum speed of $4\,\mathrm{m\,s^{-1}}$ described in the analysis overview is imposed here as in all other eastward and westward plots that follow. The southern midlatitude data are shifted by six months so that the seasons for north and south align before being merged with northern midlatitudes. The totals have been converted to monthly average number of systems per million square kilometers of each geographical region. These monthly averages for the four geographical regions appear in Fig. 4, with a logarithmic vertical scale for number density.

As expected the difference between eastward and westward occurrence density is larger for the midlatitudes: a ratio of almost 10:1 over land and 50:1 over the oceans. For the tropics strong seasonality is seen in the eastward component, which drops from May to October so that the westward–eastward ratio rises from about 2:1 to 10:1 during the extended Northern Hemisphere summer. The largest seasonal variation in number of storms is seen in the tropics for systems moving eastward, hitting a minimum for northern summer as also seen in Fig. 3. The greatest contrast between the densities of land and sea convective systems is for the rather rare westward midlatitude systems, with land–sea ratios as high as 5:1.

With this brief seasonal survey in hand, in the interests of brevity all the following analysis will either be annual averages or summer and winter comparisons.

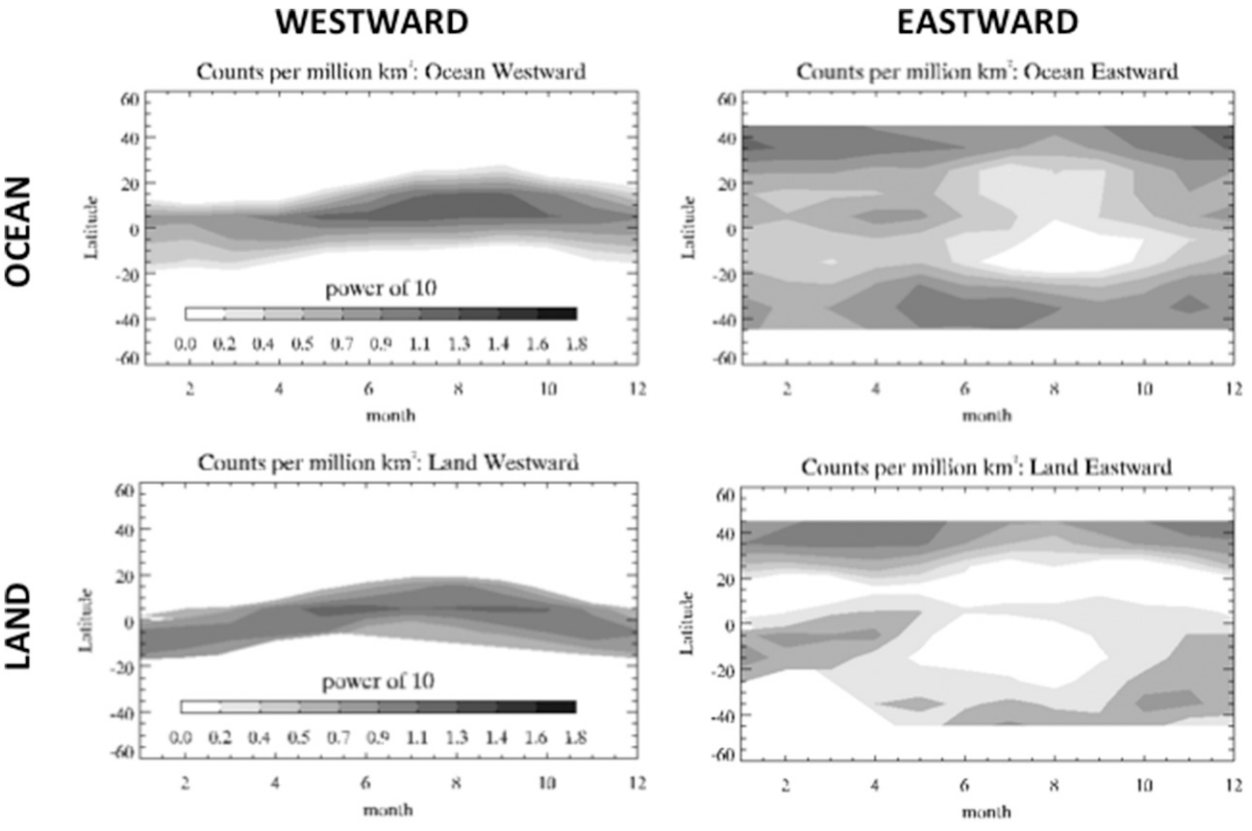

FIG. 3. Density of multiday zonally moving storms as a function of latitude and month. The scales for eastward and westward motion are the same.

b. Distributions of cloud system properties

Four properties are used to describe a cloud system life cycle: lifetime, maximum radius, minimum temperature (of the cloud-top average), and velocity as described in the dataset section above. These variables are formed into histograms for each of the four geographic regions, with results appearing in Fig. 5. All seasons are included, and all except the lifetime plot are limited to cloud lifetimes greater than 1 day. The geographic coding of the line styles is the same as for the previous figure (and will continue for the next two figures). All vertical axes are logarithmic.

The distributions of lifetimes in the top left panel of Fig. 5 have a very similar negative exponential distribution in all four geographical regions. These plots show slight curvature due to combining all seasons: when confined to a single season the histograms are very straight (not shown), showing a clear exponential distribution of lifetimes. Lifetime is the only variable that appears to have a nearly similar distribution geographically, at least for the four coarse divisions chosen for this work. The distribution over oceans decreases slightly less with lifetime than over land, so that there are more long-lived systems over oceans compared to land. This result exemplifies the need for a long data record to obtain adequate sampling of rare longer-lived systems. The lower 1-day lifetime limit for all other variables is indicated by the dotted line.

The distributions of minimum average temperature (Fig. 5, top right) show that both land and sea in the tropics have colder cloud tops than in the midlatitudes, as expected from the deeper convection associated with higher tropopause height in the tropics. Yet very little difference is seen between the land and sea distributions in each latitude zone, which may seem to contradict the observation that cloud-top temperatures over land are on average 13 K colder than over oceans (Rossow and Schiffer 1999). The discrepancy is due to selecting life cycle extrema from deep convection only versus a survey of all cloud types; also, oceans have more low-level clouds than land. In this study involving only cold clouds this major difference is filtered out of the average.

The sudden drop on the left of the radius plot (Fig. 5, bottom left) only appears when systems with lifetimes shorter than 1 day are excluded, indicating a physical lower limit of about 200-km equivalent radius for multiday systems. For the remainder of the distribution

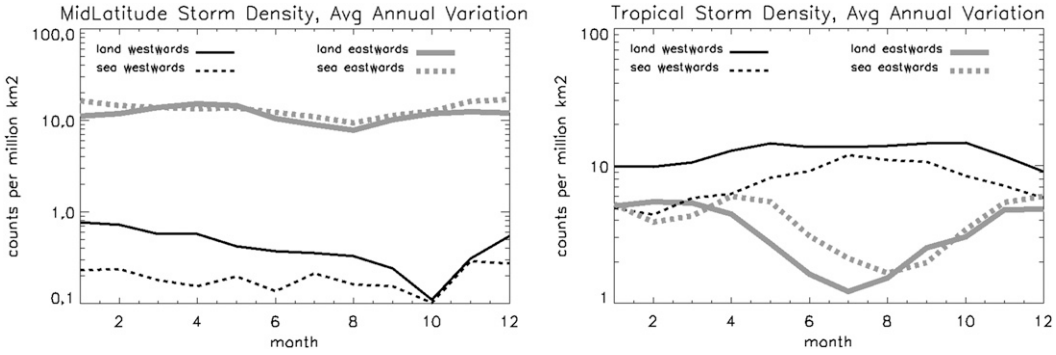

FIG. 4. Monthly variation in multiday cloud-track density per geographical region for (left) midlatitudes and (right) tropics. Land (ocean) values are shown by solid (dotted) lines; westward (eastward) motion is denoted by thin black (thick gray) lines.

above 200-km radius the oceans exhibit the same slope regardless of latitude belt, yet the midlatitude land distribution falls off with radius noticeably faster than in the tropics (Machado and Rossow 1993). Ocean regions exhibit a nearly exponential fall in population with radius as indicated by the nearly straight lines.

We note that the power-law distribution for cloud radius expected from the fractal nature of clouds (Wood and Field 2011; Machado and Rossow 1993; Cahalan and Joseph 1989) need not apply to this case for two reasons. The first is that roughly two-thirds of the data are cloud tribes with more than one concurrent cloud cell, so the equivalent radius is calculated from the summed area. A test of eliminating all but the simple cloud families does bring the distribution closer to a power law (not shown). The second difference is that this distribution picks out the largest radius from the entire cloud tribe lifetime, which is not equivalent to the ''snapshot'' distribution used in other studies that captures all cloud cells in the domain at any given

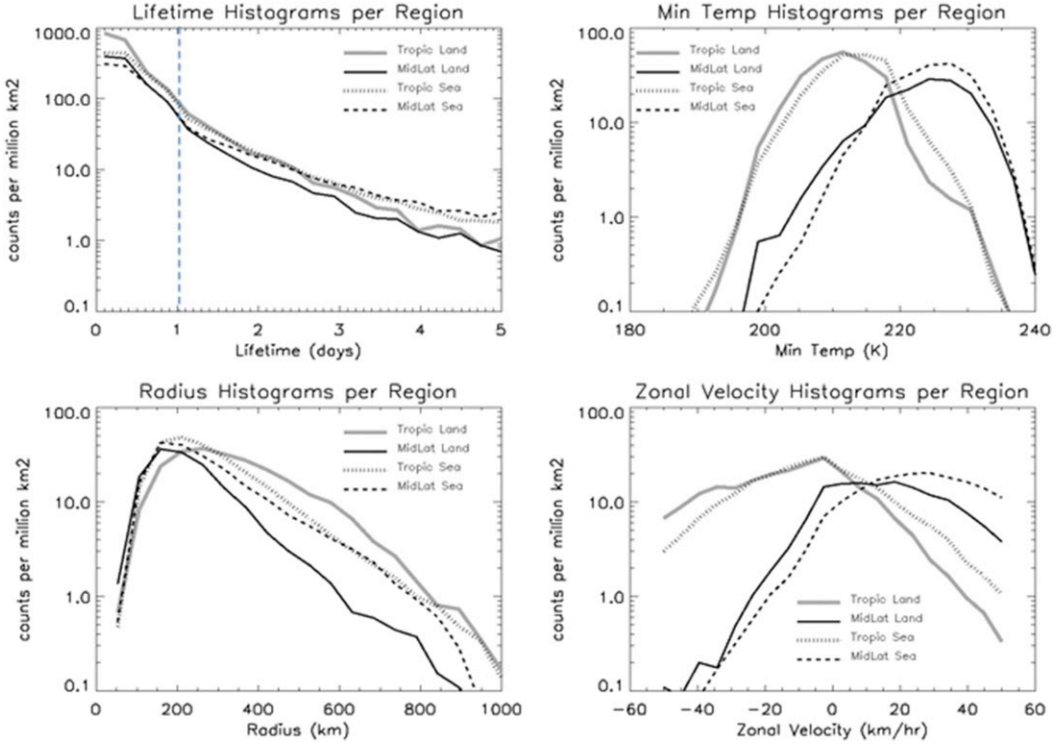

FIG. 5. Histograms of MCS characteristics, for all four seasons combined. Land (ocean) regions are shown by solid (dotted or dashed) lines . Midlatitudes are black lines, and tropics are gray lines.

TABLE 1. Average characteristics of all MCSs by geographical region, further subdivided by single-day or multiday lifetimes. Values in parentheses are subdivided by velocity for systems moving eastward/westward.

	Lifetime (days)	Zonal velocity (km h^{-1})	Max radius (km)	Avg cloud-top T (K)
All systems				
Midlatitude land	1.25 (1.30/0.97)	22.5 (29.1/−14.2)	229 (232/213)	225.9 (225.7/226.7)
Midlatitude sea	1.56 (1.63/0.90)	32.2 (36.9/−15.7)	267 (271/226)	227.2 (227.2/227.6)
Tropical land	1.01 (1.00/1.01)	−9.5 (18.2/−24.8)	273 (265/277)	214.1 (214.8/213.8)
Tropical sea	1.49 (1.53/1.46)	−2.6 (19.9/−20.2)	264 (270/260)	216.4 (217.2/215.8)
Single-day lifetimes				
Midlatitude land	0.60 (0.61/0.55)	23.4 (32.5/−16.9)	187 (188/185)	226.8 (226.7/227.5)
Midlatitude sea	0.60 (0.61/054)	31.9 (39.5/−18.1)	203 (202/204)	228.6 (228.6/228.5)
Tropical land	0.55 (0.54/0.55)	−9.5 (20.8/−26.9)	217 (212/220)	215.2 (215.7/214.9)
Tropical sea	0.63 (0.62/0.63)	−2.7 (23.0/−22.9)	198 (197/198)	218.4 (219.1/217.8)
Multiday lifetimes				
Midlatitude land	2.09 (2.12/1.87)	21.3 (25.0/−8.4)	284 (285/275)	224.6 (224.6/224.7)
Midlatitude sea	2.56 (2.59/1.97)	32.5 (34.5/−8.3)	334 (336/291)	225.8 (225.8/225.1)
Tropical land	1.95 (2.02/1.91)	−9.6 (12.3/−20.6)	385 (382/387)	211.9 (212.7/211.5)
Tropical sea	2.44 (2.54/2.36)	−2.5 (16.5/−17.3)	337 (350/327)	214.2 (215.0/213.7)

time, including cloud sizes throughout the whole life cycle.

When binned by velocity (Fig. 5, bottom right) the differences between the midlatitudes and tropics become evident: both distributions are asymmetric around zero velocity, with the distribution falling off at different rates depending on whether the motion is the same direction or opposite to the zonal average velocity. In the midlatitudes the fall off upstream with velocity against the mean flow is steeper than the equivalent in the tropics, matching the differences seen in Fig. 4.

Table 1 lists average values of all variables in the geographic regions. These are lifetime extremes of convective systems only, moving predominantly east or west. Lifetimes are split into greater and less than 1 day. As expected, multiday systems are typically larger and colder than single-day systems. The greatest geographical differences are higher speeds over midlatitude oceans compared to land, and colder, higher clouds in the tropics. The low average tropical speeds indicate a larger fraction of eastward velocities that offset the predominant westward velocities, more so over oceans than land. Reasons for regional radius differences are not physically obvious, although single-day and multiday systems follow the same pattern.

When split into eastward or westward-moving systems, the most obvious differences are in the speeds: with eastward systems moving faster than westward systems by a factor of almost 2 for midlatitude single-day systems, increasing to a factor of 3 or 4 for multiday systems. The tropical changes are much smaller with directions reversed. Other than speed the only noticeable difference is for size in the midlatitudes. The difference is confined to the average over ''all systems,'' which suggests that what is actually being affected is the distribution between multiday systems and single-day systems, with the larger multiday systems predominating for midlatitude eastward motion.

c. *Ratios of eastward to westward number of convective systems*

For Fig. 6 velocity is used to separate cloud systems into eastward or westward motion categories: histograms are formed for each variable as in Fig. 5, and the histograms divided to get the ratio of one direction to the other. In the midlatitudes the division is eastward and westward because of the average flow; in the tropics it is reversed so the ratio is always greater than unity.

The lifetime and maximum radius results are similar in that the midlatitude ratios are between 1 and 5 for short lifetimes, increasing as the plotted variable increases. The tropical values are comparatively flat and vary between 2 and 0.5, with a slight decreasing trend. This should be compared to the observation by Nakazawa (1988) that during MJO events larger structures tend to propagate opposite to the cloud-scale structures. The temperature values are not so easily described except for the midlatitude oceans, which maintain a ratio of about 10:1 regardless of cloud-top temperature, although life cycle minimum cloud-top temperature averages warmer than 205 K are rarely seen in the tropics for multiday systems. These ratios are comparable to what was seen in Fig. 4, which was not subdivided by cloud properties.

In summary the larger or longer lived a system is, the more likely it is to be moving in the expected direction in the midlatitudes, but in the tropics a slight tendency is seen for the number of eastward-moving systems to increase with size and lifetime.

In the next few sections the relationships between the cloud system variables of Figs. 5 and 6 are investigated

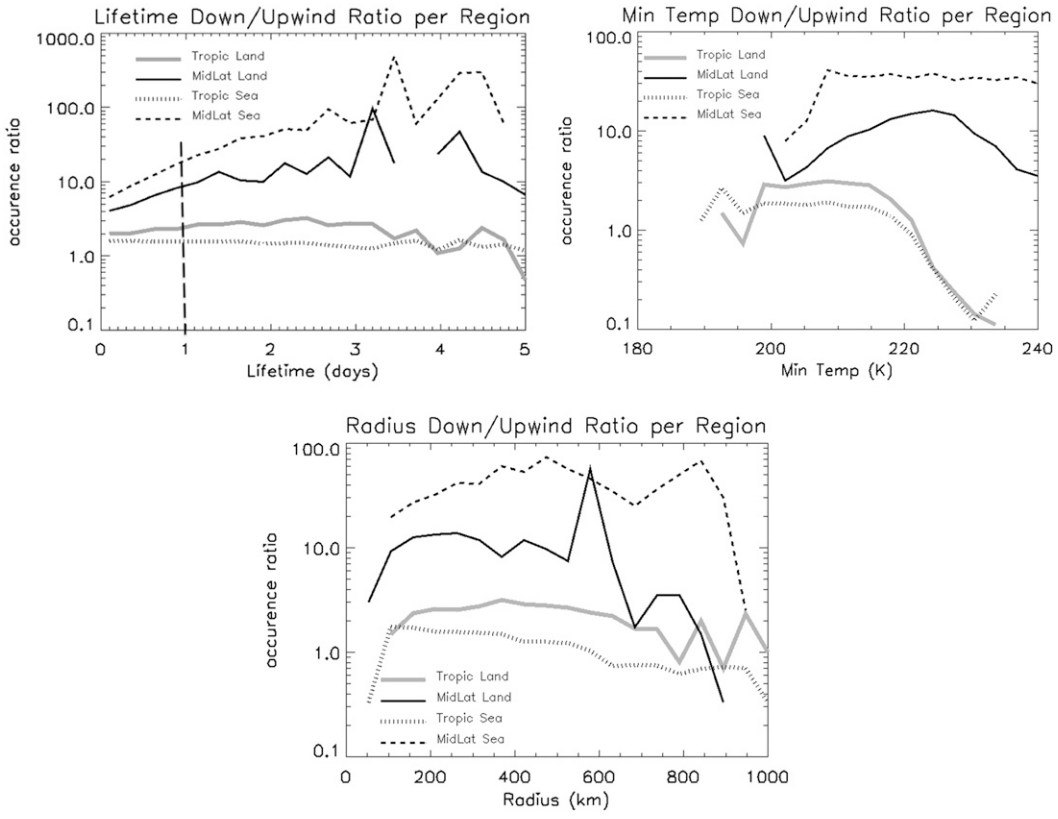

FIG. 6. Ratios of histograms for motion in the same or opposite direction as the annual zonal mean flow. Ratios greater than 1.0 mean there are more occurrences in the same direction as the mean flow. Land (ocean) values are shown by solid (dotted or dashed) lines. Midlatitudes are black lines, and tropics are gray lines. Only multiday systems are included for the radius and temperature plots. These are annual averages.

for the four geographical regions, with seasonality portrayed by comparing winter to summer months by hemisphere as described in section 2.

d. Maximum radius and lifetime

The relationship between lifetime maximum area and duration has been noted and analyzed most extensively in a series of papers by Machado and others [Machado and Rossow 1993; Machado et al. 1998; Machado and Laurent 2004; see also Pope et al. (2008)], although the datasets used are geographically limited and the systems studied rarely had lifetimes that exceeded 1 day. The maximum radius was found to be roughly linear with lifetime. In the following sections for display purposes the lifetime data (available at discrete 3-h intervals) have had random dithering applied to reduce overlaps between multiple points with the same lifetimes.

Qualitatively examining the scatter diagrams for the four geographical regions in Fig. 7 (top four panels for summer and bottom four panels for winter), the data seem to consist of a dense nucleus at 1–2 days that transitions into a halo of scattered points at longer lifetimes, in line with observations in the western Pacific (Pope et al. 2008). In the midlatitudes the nucleus and halo appear to have roughly the same slope of radius versus lifetime, but in the tropics this halo appears to favor lower radii, reducing the slope of a least squares fit as shown by the dotted lines that are a fit to the first 3 days of lifetime. Tropical land is the outlier in the maximum radius versus lifetime relationship, having the highest radius–lifetime ratio both for all lifetimes and short-lived systems. The greatest seasonal change to the slope is over land, for which the radius increases more with lifetime in the summer than in the winter.

Machado et al. (1998) found that the maximum radius increased at a rate of roughly 100 km day^{-1} of system duration, although their dataset rarely included system lifetimes exceeding 1 day, and combined data over North and South America. Our dataset with lifetimes longer than 1 day exhibits a similar joint tendency, although the slope seems to reduce with lifetime. The spread of data in both Machado et al. (1998) and Pope

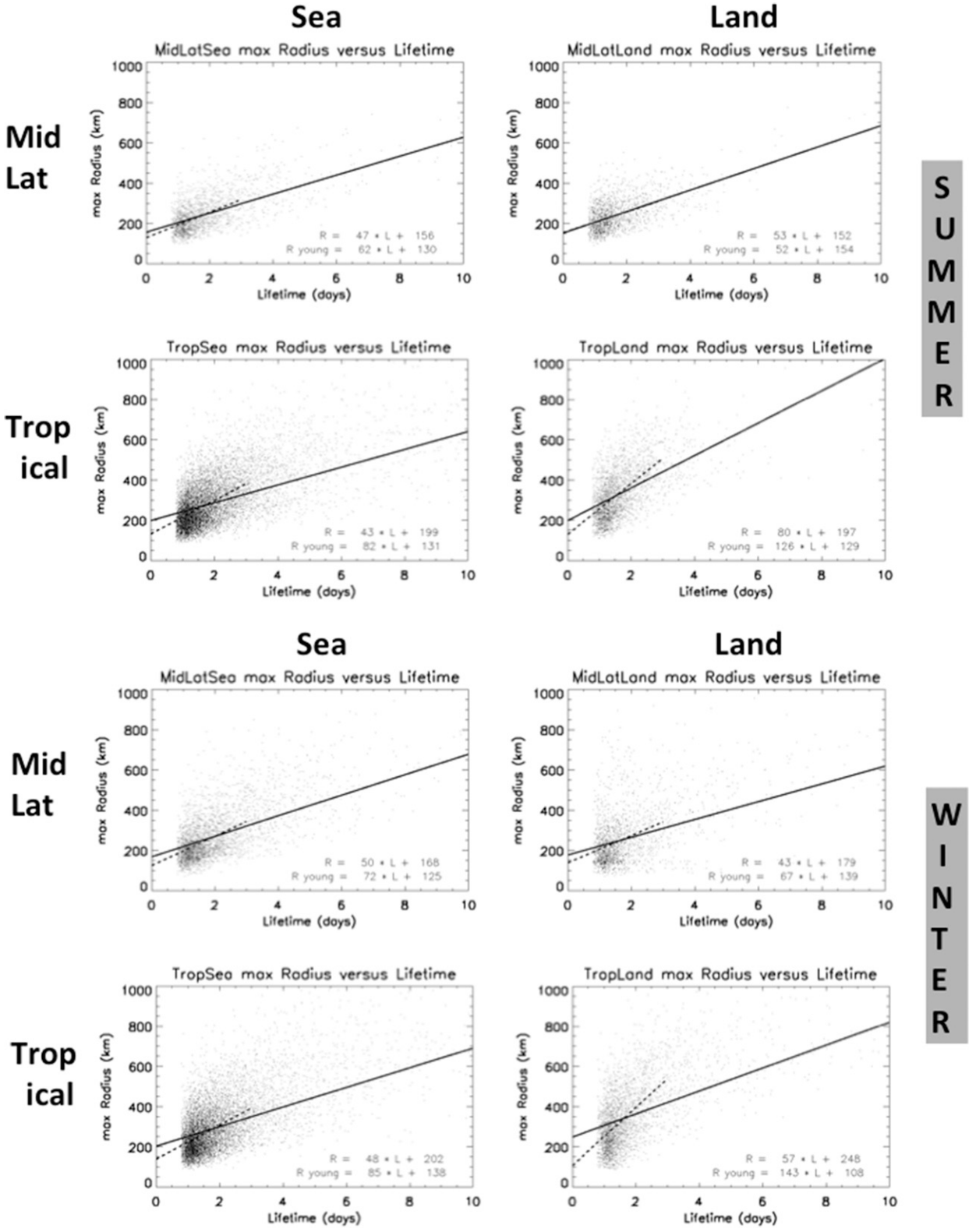

FIG. 7. Relationship between cloud system maximum equivalent radius and lifetime: (top) summer for midlatitudes and tropics and (bottom) winter for midlatitudes and tropics over (left) sea and (right) land. The solid line shows the least squares fit. ''R young'' is the radius fit to the first 3 days only (dotted line).

et al. (2008) increased with system lifetime, as does ours. As our data include much longer lifetimes with associated increase in scatter, we note that any projections, and most especially the linear projections of Fig. 7, are of limited applicability.

The coupling between maximum radius and lifetime means that both variables exhibit similar behaviors with respect to zonal velocity, as seen in the next section.

e. *Maximum equivalent radius and lifetime versus zonal velocity*

Figure 8 shows scatterplots of the maximum equivalent radius of each convective system's life cycle versus the zonal velocity of the system for summer (Fig. 8, top four panels) and winter (Fig. 8, bottom four panels). The four geographic regions are compared, and the tendency of the midlatitudes to be heavily weighted toward the eastward-moving systems versus the lightly westward-weighted tropics is immediately apparent. The number of systems moving in each direction is shown at the bottom of each plot. In the midlatitudes we see eastward–westward ratios ranging from 8:1 over land to 20:1 over oceans. In the tropics the ratio ranges from 1.3:1 over ocean to 2:1 over land. Looking at the midlatitudes it is clear that the smaller systems have a greater fraction moving eastward compared to the larger systems, as might be expected for small systems responding to cyclonic motion rather than producing it.

The gray lines show the average velocities for each radius bin. The seasonal differences in velocity distributions are stark: there is a shift to westward-moving systems for all regions in the summer compared to the winter. In winter the tropical velocities are from nearly average to zero, jumping to 10–20 km h^{-1} average for westward motion in the summer. In midlatitude summer over the oceans the average velocity is nearly constant toward the east at about 20 km h^{-1} for all radii; in the winter the systems with radii above 200 km move about 10 km h^{-1} faster on average than in summer. Over midlatitude land the average eastward speeds first increase with size up to 30 km h^{-1} at about 300-km radius, and then drop to about half the speed.

The change of average velocities with radius as shown by the gray lines may be suspect given the scatter shown in Fig. 8. To test the statistical significance, radius bins of 50–150, 250–350, and 450–550 km were selected for a Student's *t* test comparison at the 95% confidence level. All bins were compared to the lowest radius bin: a 0 appears to the left if there is no statistical difference between the averages, and a 1 appears if there is. Clearly there is no difference between the lowest bin and itself, therefore a 0 appears. In most panels the average velocity increases with radius, and the *t* test results show these differences to be significant (a 1 appears to the left). Over the tropical oceans, in contrast, the average velocity first increases slightly with radius, then decreases back to zero. The *t* test confirms that the small initial increase is significant (with a 1), and the return to zero velocity for both large and small systems is in agreement. The discussion in the preceding paragraph is thus statistically relevant.

Figure 9 plots lifetime as a function of velocity in the same manner of Fig. 8. Given the relation between maximum radius and lifetime seen in Fig. 7, it is no surprise that lifetime versus zonal velocity plots in Fig. 9 are very similar to Fig. 8, although the differences between average velocities at different lifetimes are unlikely to be statistically significant. Midlatitude land in both summer and winter shows a significant tendency for long-lived systems to have a slower eastward velocity.

f. *Cloud-top temperature versus zonal velocity and radius*

As discussed in the data section above, throughout this paper temperature refers to cloud-top average temperature over a cloud cell at any given time. All geographic regions exhibit an ellipsoidal distribution of lifetime minimum temperature versus zonal velocity. The lack of inclination of this ellipsoid indicates the two variables are not correlated, so the plot is omitted.

Figure 10 shows plots of the lifetime minimum of cloud-top average temperature against lifetime maximum cloud radius. For this figure the vertical axis of temperature is inverted so that higher (and colder) clouds appear higher on the plot. Since data are stored in integer counts instead of continuous values, for clarity the temperature values in this plot have had random dithering over a 1 K range applied to reduce overlap between points. The lifetime minimum of the average cloud-top temperature tends to increase with maximum equivalent radius, but a close look reveals scattered cold points at 200 K in the midlatitudes and 180 K in the tropics, which is 10–15 K cooler than the average tropopause temperature in each region (Seidel and Randel 2006), indicating penetrating convection (Rossow and Pearl 2007). The relationship between lifetime minimum temperature and maximum radius has been noted before (Machado et al. 1998) and is used for nowcasting purposes (Vila et al. 2008) and rainfall estimation (Delgado et al. 2008). It indicates increasing frequency of penetrating convection (Rossow and Pearl 2007) as cloud size increases. The rather weak relationships we see here may be due to the use of multiday systems as opposed to the typically shorter lifetimes seen in other studies (Pope et al. 2008). The largest seasonal changes in these plots are

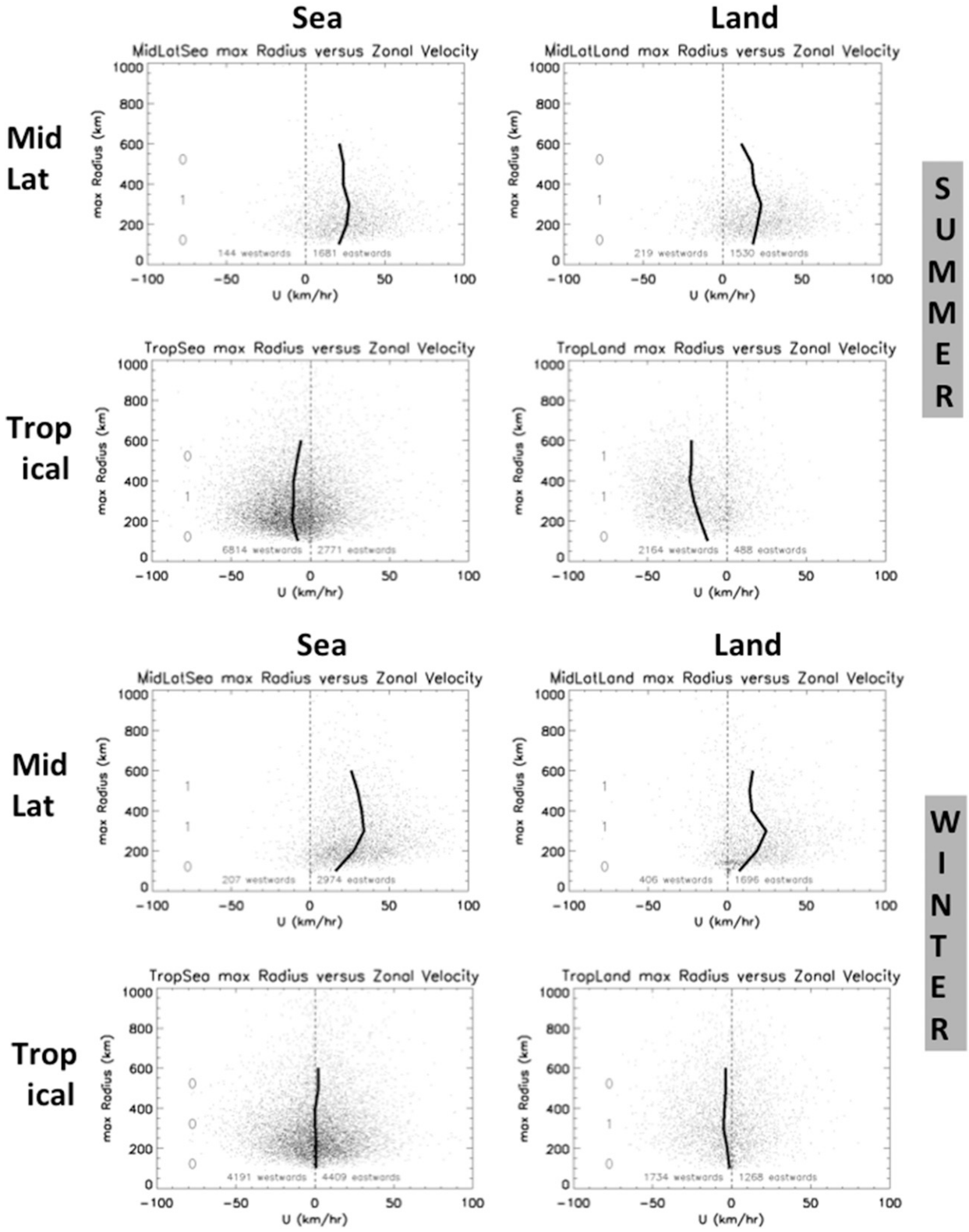

FIG. 8. As in Fig. 7, but for maximum equivalent radius during lifetime plotted vs zonal velocity. The gray line shows average velocity for each radius bin. The numbers on the left inside each panel are explained in the text.

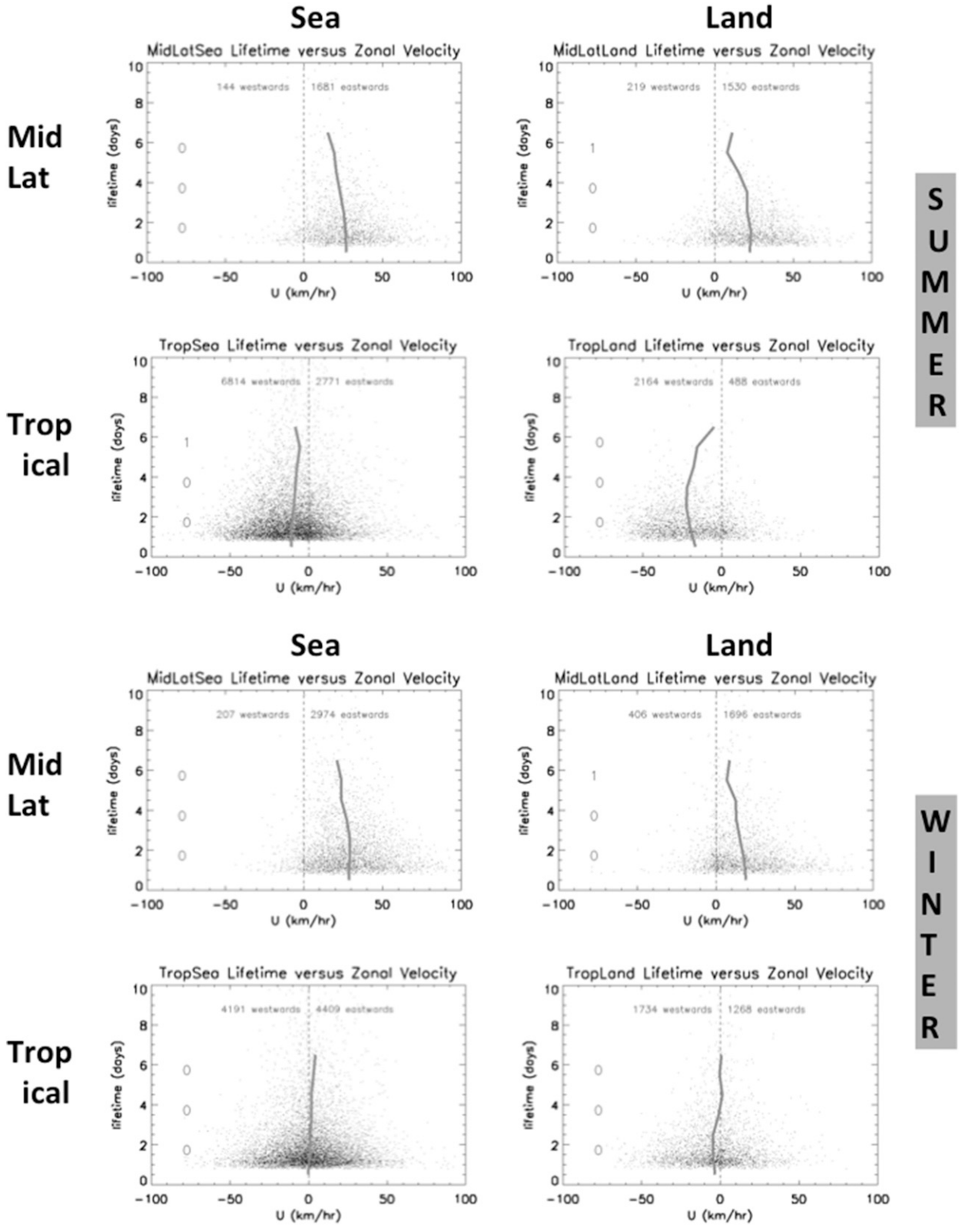

FIG. 9. As in Fig. 7, but for lifetime plotted as a function of velocity. The gray line shows average values of velocity at each lifetime. The numbers on the left inside each panel are explained in the text.

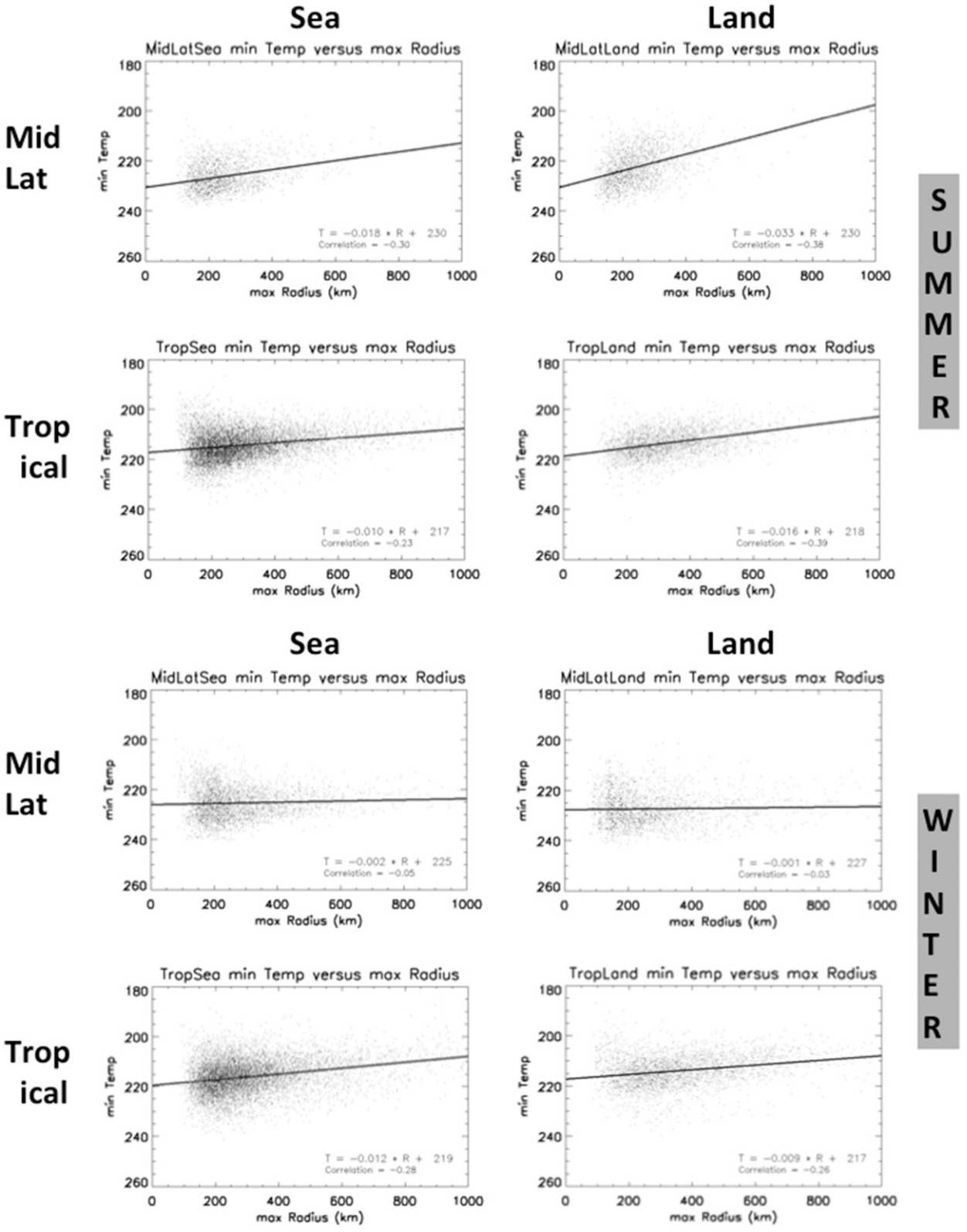

FIG. 10. As in Fig. 7, but for scatterplots of lifetime minimum cloud-top temperature vs lifetime maximum equivalent radius. Note that temperature (K) on the *y* axis is inverted.

TABLE 2. Life cycle variables and plotting style for Figs. 11–14.

Variable	Line style	Description
Radius	Black line	Calculated from the areas of all concurrent cloud cells added together, treated as a circle. Plotted as radius in kilometers scaled by 1/100.
Temperature	Gray line	Average cloud-top temperature of all concurrent cloud cells in the tribe at the time. Plotted as 235 − T (K) (so that colder temperatures are higher; e.g., 235 − 220 = 15 K).
Family count (N family)	Dashed line	Number of families in the tribe at the given time; equals the number of concurrent cloud cells.
Convective core fraction (CCfrac)	Dashed-dotted line	Fraction of all cloud area that is colder than 220 K. Plotted as CCfract × 10 (e.g., 50% × 10 = 0.5 × 10 = 5).
Convective core count (CCnum)	Dotted line	The number of contiguous areas with pixels colder than 220 K. Plotted as CCnum/4 (e.g., for CCnum = 10, 10/4 = 2.5).

seen in the midlatitudes. Over land the temperature is nearly flat with system size in the winter, but cools more strongly with radius in the summer. There is also a greater spread in system sizes in the winter. This pattern is reversed over the midlatitude oceans. Over tropical land the pattern is similar to the midlatitudes but less pronounced.

The tendency of longer lifetimes to be associated with larger radius and cooler cloud-top temperatures makes it tempting to classify longer-lived systems as hurricanes and typhoons, and our database shows an average of 78 storms per year with effective radii >500 km and lifetimes >1 day, which compares favorably with the NCDC average of 86 tropical cyclones per year (Henderson-Sellers et al. 1998). This conflicts with Romps and Kuang (2009, hereafter RK09), who demonstrate by location matching with NCDC data that only 15% of large tropical systems in the ISCCP database are associated with tropical cyclones. Their dataset of about 130 000 ISCCP convective systems with effective radii larger than 500 km is 72 times larger than our 1800 convective tribes and families with a maximum radius greater than 500 km. Our much smaller dataset arises mainly because our approach reduces each family of clouds to a single life cycle value. Further reductions occur when our method eliminates overlapping families that remain in the original dataset after two families merge, restricts to lifetimes longer than 1 day, and filters out slow-moving or north–south-moving systems. A convective system is only classified as a tropical cyclone during part of its life cycle, so counting each viewing separately as RK09 did will yield a higher count of noncyclone systems compared to our method of using a single value to represent an entire life cycle.

Because of the rough relationship between lifetime and maximum radius (Fig. 7), the equivalent plot of lifetime and minimum average temperature resembles Fig. 10, so is not presented.

g. *Multiday averaged life cycles*

Convective systems of equal lifetimes may be averaged together to represent the life cycle (Machado and Rossow 1993; Machado et al. 1998; Machado and Laurent 2004; Pope et al. 2008). As lifetimes surpass 1 day the number of systems decreases quasi-exponentially (Fig. 5), then it becomes difficult to find a dataset for any given lifetime that is large enough to provide statistically meaningful averages. This can be partially mitigated by coarsening the time step from 3 to 12 h, and binning together systems that begin or end in the same day or night period, that is, effectively increasing the dataset for each lifetime by a factor of 4. To further increase the dataset while keeping similar solar cycles, spring and fall months will be averaged together.

Lag-correlation tests matched cloud-top temperature with local solar zenith angle for offsets of 6 h in either direction. Accordingly for each cloud system the 3-h time step was located that best matched the local solar zenith each day, and then points 6 h before and after this time were retained for morning and evening snapshots to capture maximum and minimum temperatures. The focus on spring and fall in a sun-locked time scheme means that all convective systems in each latitude band were experiencing similar diurnal forcing. Systems in each geographical region with equal numbers of morning and evening snapshots are grouped, and averages formed at each time step. Table 2 describes the variables averaged by this method, and the plot styles. The family and tribe terminology has been described in the dataset section. Lone families have been removed in order to accentuate the life cycle of contemporaneous families and merges.

Figures 11–14 cycle through the regions, looking at 2- and 5-day life spans, divided into eastward and westward motion. All scales are the same, but note (as described in Table 2) that the physical values have been scaled or

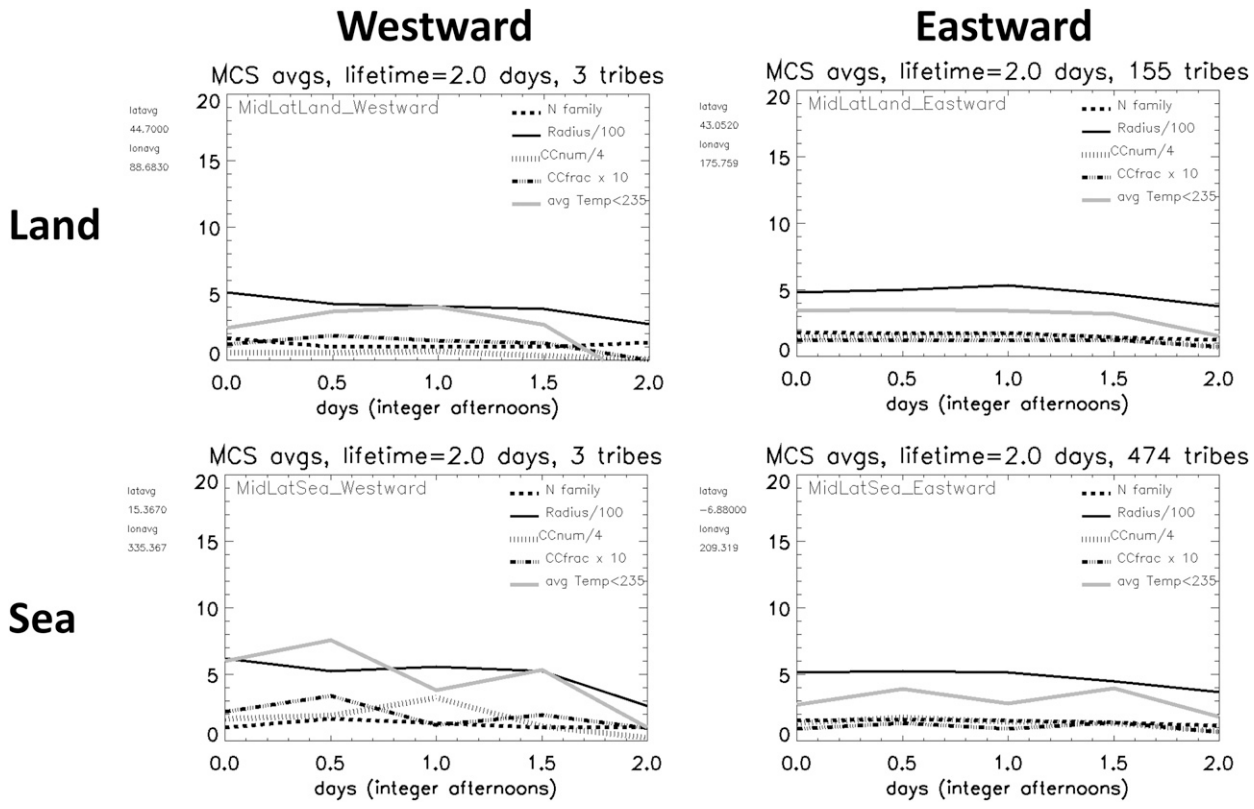

FIG. 11. Midlatitude average life cycles for systems with 2-day lifetimes (see Table 2).

shifted to fit a common axis. Temperatures are inverted so that cooler is higher in the plot. The use of dashed lines for the number of families and dotted lines for the number of smaller convective cores is intended to be suggestive for easier interpretation. Since most systems were initially detected in the afternoon, the plots begin with the first afternoon as zero, and thereafter afternoons are integer and mornings are half integer.

Because of the strict criterion on velocities as well as lifetimes, many of the categories in Figs. 11–14 are not well populated. If we focus attention on those that are, we can make several life cycle observations:

- The diurnal cycle of land and oceans is reversed. Over land, cloud tops for deep convection are colder and higher in the afternoons; over oceans they are colder and higher in the mornings. This is not a new observation (Gray and Jacobson 1977; Mapes and Houze 1993; Chen and Houze 1997; Soden 2000) but may come as a surprise to those who study convection over land. Modeling studies suggest that the diurnal cycle over ocean is due mainly to large-scale radiative cooling (Miller and Frank 1993; Liu and Moncrieff 1998), with controlled modeling experiments by Tao et al. (1996) indicating that this is due to the increase in relative humidity rather than atmospheric column destabilization.
- The equivalent radius has a weak diurnal cycle. The radial growth weakly reflects vertical growth as shown by cloud-top temperature diurnal cycle over land, with a much weaker negative response over oceans. The diurnal changes are small compared to changes over the lifetime.
- The equivalent radius tends to change by less than 50% over the life cycle. This is in agreement with previous studies that show area rarely increasing above a factor of 2, although such analyses rarely extended beyond 1-day system duration (Machado et al. 1998; Machado and Laurent 2004; McAnelly and Cotton 1989).
- Both convective fraction and average cloud-top temperature oscillate diurnally about a stable average. The convective fraction is defined by a fixed temperature threshold chosen to ensure that anvils will be predominately warmer, so that convective fraction indicates strong penetrative activity above the anvil (Fu et al. 1990). Our multiday observations

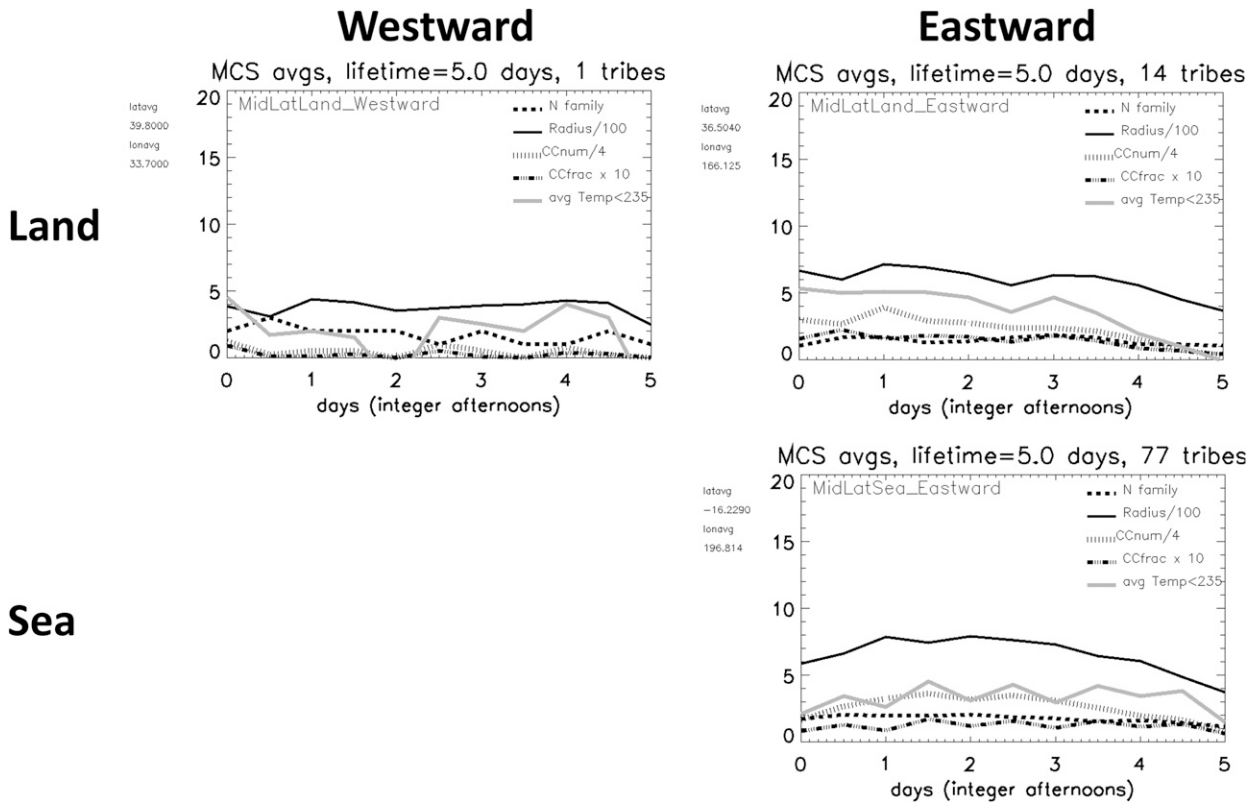

FIG. 12. Midlatitude average life cycles for systems with 5-day lifetimes (see Table 2). No data is available for westward-moving systems over the ocean.

somewhat conflict with earlier studies (Machado et al. 1998) for life cycles less than 1 day, but showed convective fraction decreasing and temperature warming with time. The conflict is resolved by the difference in time scale: It is only after the first day of growth that the character of multiday convective systems stabilizes on average, until the decay on the last day (see also Pope et al. 2008).

- The average number of families in a tribe remains close to 2 throughout the life cycle. Given that the average tribe has 4.5 merges spread throughout its life cycle (Fig. 2), this paints a picture of a main cell with ancillary cells appearing and merging with it in succession. Longer life cycles over tropical land tend to be more variable. Note that lone families (no splits or merges) were excluded from these particular plots.

5. Discussion

a. Eastward- versus westward-moving systems

Under the assumption that the physical mechanism in each region causing long-lived convective systems to move eastward is different from that of westward motion, we might expect that the scatterplots of velocity versus other variables (Figs. 8 and 9) would show a clustering effect divided between the two directions. Instead we see smooth monomodal distributions. This suggests either that variables chosen do not reflect the propagation mechanism or that, since the velocities fall on a continuum, the mechanisms behind them are also continuous rather than discrete. The first case might refer to the various global-scale waves—convectively coupled Kelvin, Rossby, and gravity waves that fall into easily discernable propagation speeds (Wheeler and Kiladis, 1999); but instead we see a smooth continuum of cloud propagation speeds indicating no direct connection between cloud and wave speeds. The propagation of the Madden–Julian oscillation may be an example of the second case: the large-scale divergence in upper-level winds associated with it has been shown to always be present (rather than ''off or on''), but with varying amplitude (Tromeur and Rossow 2010). A more definitive test of whether the MJO affects the MCS properties is described in the next section.

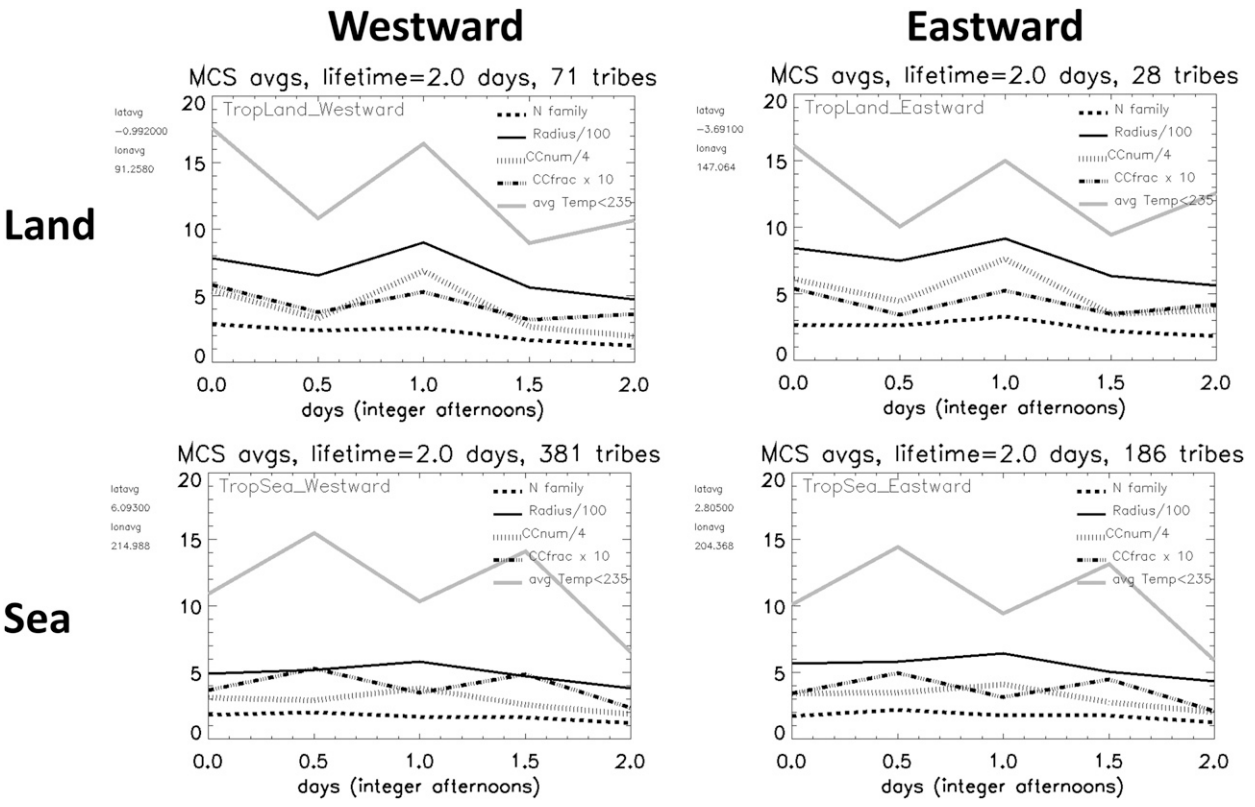

FIG. 13. Tropical average life cycles for systems with 2-day lifetimes (see Table 2).

But are life cycles different for eastward versus westward propagation? The only obvious directional differences in the life cycle plots of Figs. 11–14 are over the tropical oceans, where the westward life cycles show colder cloud tops (and hence higher convective fraction, see the discussion in section 4g) than the eastward life cycles, a difference of 2–3 K. Nearly all tropical ocean systems show this trend; the 2-day system shown is one of the few that did not. Yet for the 5-day system the large ensemble of 345 westward versus 170 eastward systems lends weight to this observed difference. This is not likely to be due to a difference in geographical location, for the average difference in latitude between the tropical eastward and westward systems is less than 1°, too small to produce a 2 K surface difference in the warm tongue of the Pacific (Reynolds and Smith 1995) where much of the eastward propagation is expected to occur. It appears that westward systems in the tropics are slightly but significantly more developed than the eastward counterparts.

b. *Is the MJO reflected in individual cloud systems?*

Part of the reason the MJO may not be apparent in this work is the use of the entire latitude bands, obscuring the signal most strongly observed in the Indian Ocean and tropical western Pacific. A test was conducted by restricting the radius versus velocity plots of Fig. 8 to the Indian Ocean and tropical Pacific (15°N–15°S, 80°E–180°), avoiding major landmasses. The data were separated into a set with high and low amplitudes of the MJO index (Hendon–Wheeler index >1.1 or <0.9) for phases 3–6 of the MJO, corresponding to the Indian Ocean–western Pacific region. No significant differences were seen between the plots, so they are not shown. The lack of a change in MCS properties is not surprising given previous work that shows the MJO modulates the ratio of occurrence of organized and disorganized convection rather than introducing new weather states (Tromeur and Rossow 2010).

To investigate alternate mechanisms for eastward propagation in this region, Fig. 15 shows cloud system radius–velocity plots for the four seasons. The only clearly unique season is Northern Hemisphere spring, for which large systems have an average tendency to propagate eastward, and it is a statistically significant trend. Since the previous test demonstrated this is not due to the MJO, we see that such behavior must be attributed to other influences such as monsoons (Pope et al. 2008).

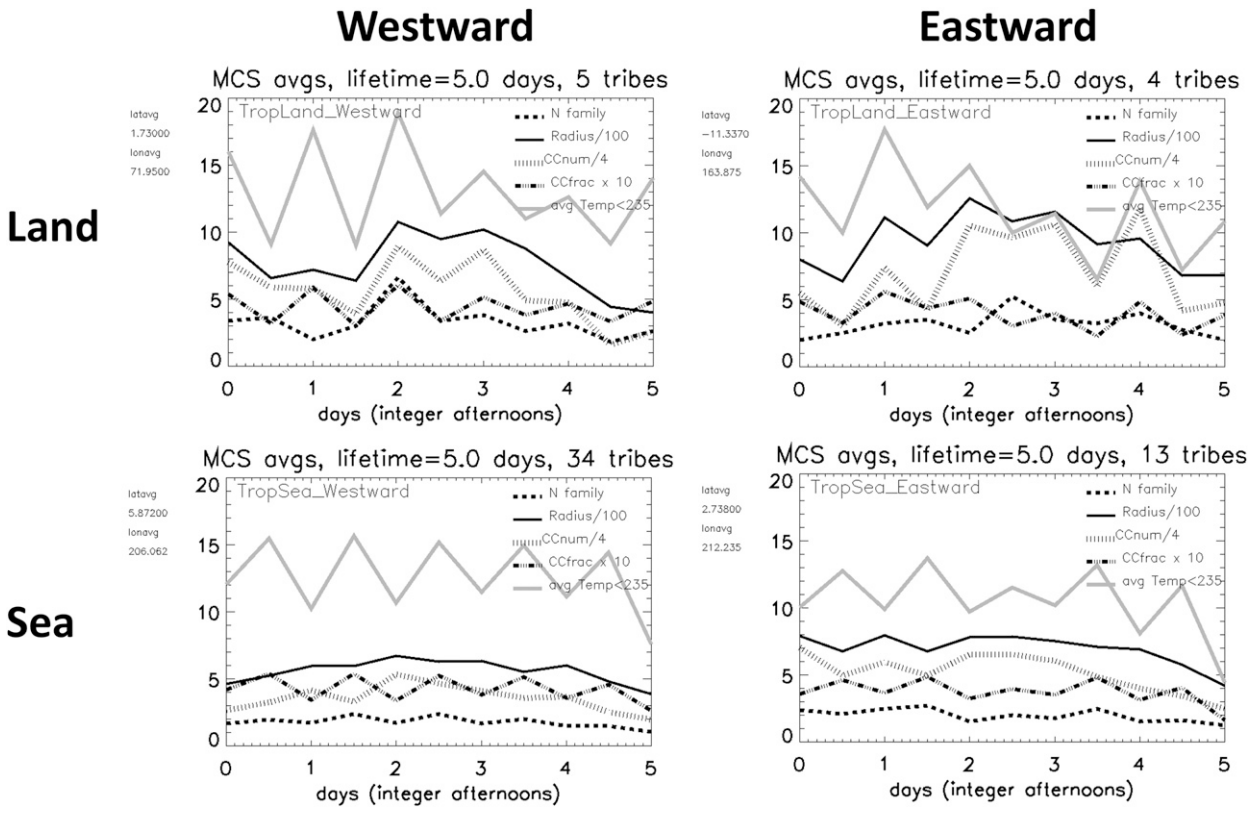

FIG. 14. Tropical average life cycles for systems with 5-day lifetimes (see Table 2).

6. Conclusions

This first study using global statistics of multiday mesoscale convective systems filters the dataset into subsets that are moving predominantly eastward or westward, and into four regions: land and ocean in midlatitude and tropical zones. Given the relative rarity of long-lived systems, these statistics would not be meaningful without a multidecadal dataset such as provided by the ISCCP. Our results naturally divide into what would be expected based on past studies comprised of systems with lifetimes rarely longer than 1 day and new findings not easily obtained with the shorter datasets.

Matching observations seen for shorter systems (Machado and Rossow 1993), the following multiday life cycle variables have coupled trends: lifetime, maximum radius, and minimum cloud-top average temperature, although the relationships are much weaker than seen in the single-day counterparts with no splits or merges (Pope et al. 2008). The size distribution falls off exponentially with system area as opposed to the negative power law distribution normally observed (Wood and Field 2011; Cahalan and Joseph 1989), but this appears to be related to using lifetime maximum size as opposed to the distribution of all clouds regardless of where they are in the life cycle. The size distribution falls off much faster over midlatitude land than ocean (Machado and Rossow 1993), but the tropical and midlatitude oceans have very similar size distributions, with tropical land featuring slightly larger multiday systems (Futyan and Del Genio 2007). The lifetime distribution also falls off exponentially.

The observed tendency for tropical convective cores and anvils to maximize in the afternoon over land and the morning over ocean has been commented on before (Gray and Jacobson 1977; Mapes and Houze 1993; Soden 2000) and continues for multiday systems. In the midlatitudes we can extend that pattern over the oceans but do not see evidence for it over land, perhaps because regional variations in deep convective timing over land tends to balance in the global average (McAnelly and Cotton 1989).

Throughout the multiday cycle, the system radius tends to rise to a gentle peak then fall, with a change of about 50% (approximate doubling in area) from when the cloud cells are first registered at 245 K. A slight diurnal cycle is superimposed on this pattern. Much stronger diurnal cycles of temperature (and the related cloud anvil fraction and number) are observed, but in contrast to the radius

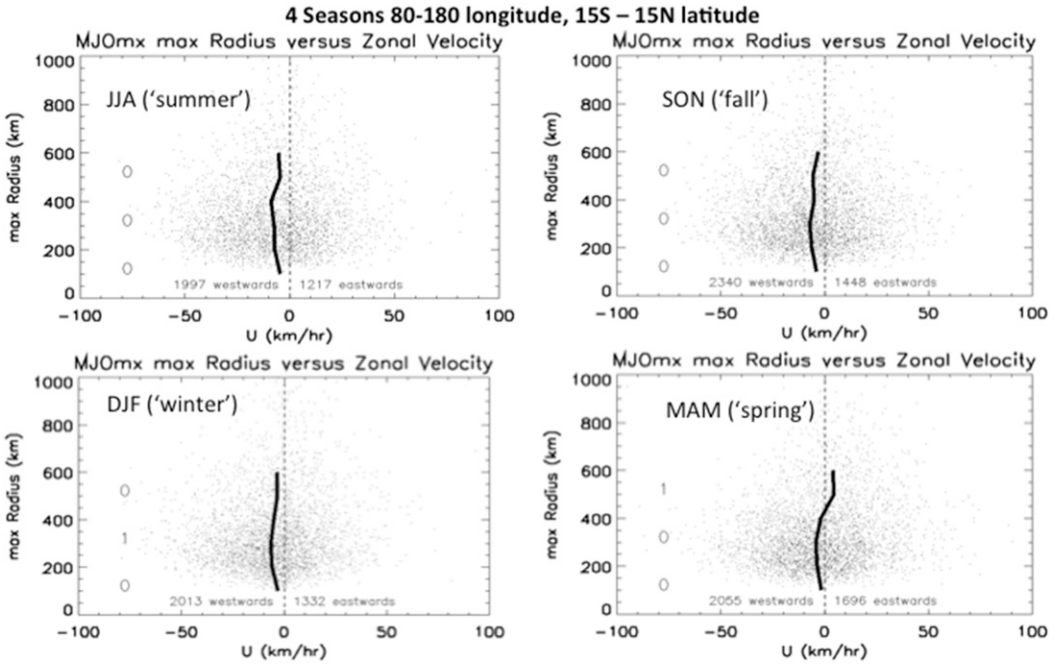

FIG. 15. Tropical Indian Ocean and western Pacific (15°S–15°N, 80°E–180°) radius vs velocity for Northern Hemisphere seasons. Numbers on the left inside each panel are explained in the text.

follow a fairly uniform diurnal cycle throughout the lifetime, endpoints excluded.

This study appears to be unique in the inclusion of split and merge statistics for multiday systems. The overall merge–split ratio is approximately 20:1, with the number of lone convective systems (no splits or merges) greater for short lifetimes (less than 1 day), crossing over to a majority of "tribal" systems (at least one split or merge) for long-lived systems with lifetimes greater than 1 day (a ratio that increases with lifetime). On average the tribal systems tend to have approximately two concurrent cells at any one time.

A significant result of this work concerns the distribution of velocities, which resemble a bell-shaped curve skewed in the direction of the zonal average motion. In the midlatitudes the center of the distribution is approximately 30 km h^{-1} eastward whereas in the tropics the distribution is centered near zero in Northern Hemisphere winter and brackets 10 km h^{-1} westward, with values higher over land than water. Although the midlatitude velocity distribution is firmly unidirectional, the tropical distribution varies from 1:1 to roughly 3:2 westward versus eastward depending on season (winter or summer). It is notable that the distributions are clearly monomodal with no obvious clustering. The absence of a clear division into more than one velocity mode provides no clear evidence that the various convectively coupled waves (Wheeler and Kiladis 1999), including the MJO, modify individual cloud behavior. Although these waves may modulate the occurrence of these multiday convective systems (Tromeur and Rossow 2010), they do not appear to otherwise influence their individual properties.

Differences emerge in the relation of convective system size to average velocity. In the midlatitudes smaller systems have a greater probability (though still very small) of moving westward, while for the tropical oceans larger systems have a slightly greater than 50% chance to be moving eastward. The size division between eastward- and westward-moving elements is most clear in the Indian Ocean during Northern Hemisphere spring. Over tropical land all systems have a greater than 50% chance to be moving eastward, but smaller systems come closest to a 50/50 split in direction.

Future work with the ISCCP CT dataset should compare single-day and multiday system properties. However, the 3-h time step in this dataset prevents investigation of the behavior of smaller convective systems, both deep and shallow, and better study of the split and merger processes. The geostationary imaging data used by ISCCP are actually available at much smaller time sampling intervals, with whole-Earth views as frequently as every 15–30 min and regional views at 5-min intervals. These data should be analyzed to characterize the properties and behavior of a more complete set of convective phenomena.

Acknowledgments. This work was made possible by NASA Grant NNX13AO39G. Additional support was

furnished by NOAA/EPP Grant NA11SEC4810004 to the CREST Institute at the City University of New York. The authors thank three anonymous reviewers for insightful comments that helped re-orient parts of this work.

REFERENCES

Cahalan, R., and J. Joseph, 1989: Fractal statistics of cloud fields. *Mon. Wea. Rev.*, **117**, 261–272, doi:10.1175/1520-0493(1989)117<0261:FSOCF>2.0.CO;2.

Carvalho, L., and C. Jones, 2001: A satellite method to identify structured properties of mesoscale convective systems based on a maximum spatial correlation tracking technique (MASCOTTE). *J. Appl. Meteor.*, **40**, 1683–1701, doi:10.1175/1520-0450(2001)040<1683:ASMTIS>2.0.CO;2.

Chang, C.-P., 1976: Forcing of Kelvin waves by tropospheric heat sources. *J. Atmos. Sci.*, **33**, 740–744, doi:10.1175/1520-0469(1976)033<0740:FOSKWB>2.0.CO;2.

——, 1977: Viscous internal gravity waves and low-frequency oscillations in the tropics. *J. Atmos. Sci.*, **34**, 901–910, doi:10.1175/1520-0469(1977)034<0901:VIGWAL>2.0.CO;2.

Chen, S., and R. Houze, 1997: Diurnal variation and life-cycle of deep convective systems over the tropical Pacific warm pool. *Quart. J. Roy. Meteor. Soc.*, **123**, 357–388, doi:10.1002/qj.49712353806.

Delgado, G., L. Machado, C. Angelis, M. Bottino, A. Redano, J. Lorente, L. Gimeno, and R. Nieto, 2008: Basis for a rainfall estimation technique using IR-VIS cloud classification and parameters over the lifecycle of mesoscale convective systems. *J. Appl. Meteor. Climatol.*, **47**, 1500–1517, doi:10.1175/2007JAMC1684.1.

Fu, R., A. Del Genio, and W. Rossow, 1990: Behavior of deep convective clouds in the tropical Pacific deduced from ISCCP radiances. *J. Climate*, **3**, 1129–1152, doi:10.1175/1520-0442(1990)003<1129:BODCCI>2.0.CO;2.

Futyan, J. M., and A. Del Genio, 2007: Deep convective system evolution over Africa and the tropical Atlantic. *J. Climate*, **20**, 5041–5060, doi:10.1175/JCLI4297.1.

Gambheer, A. V., and G. S. Bhat, 2000: Life cycle characteristics of deep cloud systems over the Indian region using INSAT-1B pixel data. *Mon. Wea. Rev.*, **128**, 4071–4083, doi:10.1175/1520-0493(2000)129<4071:LCCODC>2.0.CO;2.

Gray, W. M., and R. W. Jacobson, 1977: Diurnal variation of deep cumulus convection. *Mon. Wea. Rev.*, **105**, 1171–1188, doi:10.1175/1520-0493(1977)105<1171:DVODCC>2.0.CO;2.

Han, Q., W. Rossow, J. Zeng, and R. Welch, 2002: Three different behaviors of liquid water path of water clouds in cloud–aerosol interactions. *J. Atmos. Sci.*, **59**, 726–736, doi:10.1175/1520-0469(2002)059<0726:TDBOLW>2.0.CO;2.

Henderson-Sellers, A., and Coauthors, 1998: Tropical cyclones and global climate change: A post-IPCC assessment. *Bull. Amer. Meteor. Soc.*, **79**, 19–38, doi:10.1175/1520-0477(1998)079<0019:TCAGCC>2.0.CO;2.

Jakob, C., and C. Schumacher, 2008: Precipitation and latent heating characteristics of the major tropical western Pacific cloud regimes. *J. Climate*, **21**, 4348–4364, doi:10.1175/2008JCLI2122.1.

Jiang, X., T. Li, and B. Wang, 2004: Structures and mechanisms of the northward propagating boreal summer intraseasonal oscillation. *J. Climate*, **17**, 1022–1039, doi:10.1175/1520-0442(2004)017<1022:SAMOTN>2.0.CO;2.

Joyce, R., J. Janowiak, P. Arkin, and P. Xie, 2004: CMORPH: A method that produces global precipitation estimates from passive microwave and infrared data at high spatial and temporal resolution. *J. Hydrometeor.*, **5**, 487–503, doi:10.1175/1525-7541(2004)005<0487:CAMTPG>2.0.CO;2.

Lakshmanan, V., T. Smith, G. Stumpf, and K. Hondl, 2007: The Warning Decision Support System–Integrated Information. *Wea. Forecasting*, **22**, 596–612, doi:10.1175/WAF1009.1.

Lau, K. M., T. Nakazawa, and C. H. Sui, 1991: Observations of cloud cluster hierarchies over the tropical western Pacific. *J. Geophys. Res.*, **96**, 3197–3208, doi:10.1029/90JD01830.

Lau, N.-C., and M. Crane, 1995: A satellite view of the synoptic scale organization of cloud properties in midlatitude and tropical circulation systems. *Mon. Wea. Rev.*, **123**, 1984–2006, doi:10.1175/1520-0493(1995)123<1984:ASVOTS>2.0.CO;2.

Liu, C., and M. W. Moncrieff, 1998: A numerical study of the diurnal cycle of tropical oceanic convection. *J. Atmos. Sci.*, **55**, 2329–2344, doi:10.1175/1520-0469(1998)055<2329:ANSOTD>2.0.CO;2.

Machado, L. A. T., and W. B. Rossow, 1993: Structural characteristics and radiative properties of tropical cloud clusters. *Mon. Wea. Rev.*, **121**, 3234–3259, doi:10.1175/1520-0493(1993)121<3234:SCARPO>2.0.CO;2.

——, and H. Laurent, 2004: The convective system area expansion over Amazonia and its relationships with convective system life duration and high-level wind divergence. *Mon. Wea. Rev.*, **132**, 714–725, doi:10.1175/1520-0493(2004)132<0714:TCSAEO>2.0.CO;2.

——, W. B. Rossow, R. L. Guedes, and A. W. Walker, 1998: Lifecycle variations of mesoscale convective systems over the Americas. *Mon. Wea. Rev.*, **126**, 1630–1654, doi:10.1175/1520-0493(1998)126<1630:LCVOMC>2.0.CO;2.

Madden, R. A., 1986: Seasonal variations of the 40–50 day oscillation in the tropics. *J. Atmos. Sci.*, **43**, 3138–3158, doi:10.1175/1520-0469(1986)043<3138:SVOTDO>2.0.CO;2.

——, and P. Julian, 1972: Description of global-scale circulation cells in the tropics with a 40–50 day period. *J. Atmos. Sci.*, **29**, 1109–1123, doi:10.1175/1520-0469(1972)029<1109:DOGSCC>2.0.CO;2.

Maddox, R. A., 1980: Mesoscale convective complexes. *Bull. Amer. Meteor. Soc.*, **61**, 1374–1387, doi:10.1175/1520-0477(1980)061<1374:MCC>2.0.CO;2.

Mapes, B., and R. Houze, 1993: Cloud clusters and superclusters over the oceanic warm pool. *Mon. Wea. Rev.*, **121**, 1398–1416, doi:10.1175/1520-0493(1993)121<1398:CCASOT>2.0.CO;2.

Masunaga, H., 2007: Seasonality and regionality of the Madden–Julian oscillation, Kelvin wave, and equatorial Rossby wave. *J. Atmos. Sci.*, **64**, 4400–4416, doi:10.1175/2007JAS2179.1.

Matthews, A., 2000: Propagation mechanisms for the Madden–Julian oscillation. *Quart. J. Roy. Meteor. Soc.*, **126**, 2637–2651, doi:10.1002/qj.49712656902.

McAnelly, R., and W. Cotton, 1989: The precipitation life cycle of mesoscale convective complexes over the central United States. *Mon. Wea. Rev.*, **117**, 784–808, doi:10.1175/1520-0493(1989)117<0784:TPLCOM>2.0.CO;2.

Miller, R. A., and W. M. Frank, 1993: Radiative forcing of simulated tropical cloud clusters. *Mon. Wea. Rev.*, **121**, 482–498, doi:10.1175/1520-0493(1993)121<0482:RFOSTC>2.0.CO;2.

Moncrieff, M., 2004: Analytic representation of the large-scale organization of tropical convection. *J. Atmos. Sci.*, **61**, 1521–1538, doi:10.1175/1520-0469(2004)061<1521:AROTLO>2.0.CO;2.

Morel, C., S. Senesi, and F. Autones, 2002: Building upon SAF-NWC products: Use of the Rapidly Developing Thunderstoms

(RDT) product in Météo-France nowcasting tools. Report to EUMETSAT, 8 pp. [Available online at http://www.meteorologie.eu.org/RDT/doc/Morel2002.pdf.]

Nakazawa, T., 1988: Tropical superclusters within intraseasonal variations over the western Pacific. *J. Meteor. Soc. Japan*, **66**, 823–839.

Oreopoulos, L., and W. B. Rossow, 2011: The cloud radiative effects of the International Satellite Cloud Climatology Project weather states. *J. Geophys. Res.*, **116**, D12202, doi:10.1029/2010JD015472.

Pope, M., C. Jakob, and M. Reeder, 2008: Convective systems of the north Australian monsoon. *J. Climate*, **21**, 5091–5112, doi:10.1175/2008JCLI2304.1.

Reynolds, R., and T. Smith, 1995: A high-resolution global sea surface temperature climatology. *J. Climate*, **8**, 1571–1583, doi:10.1175/1520-0442(1995)008<1571:AHRGSS>2.0.CO;2.

Romps, D. M., and Z. Kuang, 2009: Overshooting convection in tropical cyclones. *Geophys. Res. Lett.*, **36**, L09804, doi:10.1029/2009GL037396.

Rossow, W. B., and R. Schiffer, 1991: ISCCP cloud products. *Bull. Amer. Meteor. Soc.*, **72**, 2–20, doi:10.1175/1520-0477(1991)072<0002:ICDP>2.0.CO;2.

——, and L. C. Gardner, 1993a: Cloud detection using satellite measurements of infrared and visible radiances for ISCCP. *J. Climate*, **6**, 2341–2369, doi:10.1175/1520-0442(1993)006<2341:CDUSMO>2.0.CO;2.

——, and ——, 1993b: Validation of ISCCP cloud detections. *J. Climate*, **6**, 2370–2393, doi:10.1175/1520-0442(1993)006<2370:VOICD>2.0.CO;2.

——, and R. Schiffer, 1999: Advances in understanding clouds from ISCCP. *Bull. Amer. Meteor. Soc.*, **80**, 2261–2287, doi:10.1175/1520-0477(1999)080<2261:AIUCFI>2.0.CO;2.

——, and C. Pearl, 2007: 22-year survey of tropical convection penetrating into the lower stratosphere. *Geophys. Res. Lett.*, **34**, L04803, doi:10.1029/2006GL028635.

——, A. Walker, D. Beuschel, and M. Roiter, 1996: International Satellite Cloud Climatology Project (ISCCP) documentation of new cloud datasets. World Meteorological Organization, 115 pp. [Available online at http://isccp.giss.nasa.gov/pub/documents/d-doc.pdf.]

——, G. Tselioudis, A. Polak, and C. Jakob, 2005: Tropical climate described as a distribution of weather states indicated by distinct mesoscale cloud property mixtures. *J. Geophys. Res. Lett.*, **32**, L21812, doi:10.1029/2005GL024584.

——, Y. Zhang, and G. Tselioudis, 2016: Atmospheric diabatic heating in different weather states and the general circulation. *J. Climate*, **29**, 1059–1065, doi:10.1175/JCLI-D-15-0760.1.

Rui, H., and B. Wang, 1990: Development characteristics and dynamic structure of tropical intraseasonal convection anomalies. *J. Atmos. Sci.*, **47**, 357–379, doi:10.1175/1520-0469(1990)047<0357:DCADSO>2.0.CO;2.

Seidel, D. J., and W. J. Randel, 2006: Variability and trends in the global tropopause estimated from radiosonde data. *J. Geophys. Res.*, **111**, D21101, doi:10.1029/2006JD007363.

Seo, K.-H., and K.-Y. Kim, 2003: Propagation and initiation mechanisms of the Madden–Julian oscillation. *J. Geophys. Res.*, **108**, 4384, doi:10.1029/2002JD002876.

Sobel, A., and E. Maloney, 2013: Moisture modes and the eastward propagation of the MJO. *J. Atmos. Sci.*, **70**, 187–192, doi:10.1175/JAS-D-12-0189.1.

Soden, B., 2000: The diurnal cycle of convection, clouds, and water vapor in the tropical upper troposphere. *Geophys. Res. Lett.*, **27**, 2173–2176, doi:10.1029/2000GL011436.

Tao, W.-K., S. Lang, J. Simpson, C.-H. Sui, B. Ferrier, and M.-D. Chou, 1996: Mechanisms of cloud–radiation interaction in the tropics and midlatitudes. *J. Atmos. Sci.*, **53**, 2624–2651, doi:10.1175/1520-0469(1996)053<2624:MOCRII>2.0.CO;2.

Tromeur, E., and W. Rossow, 2010: Interaction of tropical deep convection with the large-scale circulation in the MJO. *J. Climate*, **23**, 1837–1852, doi:10.1175/2009JCLI3240.1.

Tselioudis, G., W. B. Rossow, Y. Zhang, and D. Konsta, 2013: Global weather states and properties from passive and active satellite cloud retrievals. *J. Climate*, **26**, 7734–7746, doi:10.1175/JCLI-D-13-00024.1.

Vila, D., L. Machado, H. Laurent, and I. Velasco, 2008: Forecast and Tracking the Evolution of Cloud Clusters (ForTraCC) using satellite infrared imagery: Methodology and validation. *Wea. Forecasting*, **23**, 233–245, doi:10.1175/2007WAF2006121.1.

Wang, B., and H. Rui, 1990: Synoptic climatology of transient tropical intraseasonal convection anomalies: 1975–1985. *Meteor. Atmos. Phys.*, **44**, 43–61, doi:10.1007/BF01026810.

Wheeler, M., and G. Kiladis, 1999: Convectively coupled equatorial waves: Analysis of clouds and temperature in the wavenumber–frequency domain. *J. Atmos. Sci.*, **56**, 374–399, doi:10.1175/1520-0469(1999)056<0374:CCEWAO>2.0.CO;2.

——, and H. Hendon, 2004: An all-season real-time multivariate MJO index: Development of an index for monitoring and prediction. *Mon. Wea. Rev.*, **132**, 1917–1932, doi:10.1175/1520-0493(2004)132<1917:AARMMI>2.0.CO;2.

Wood, R., and P. Field, 2011: The distribution of cloud horizontal sizes. *J. Climate*, **24**, 4800–4816, doi:10.1175/2011JCLI4056.1.

Yang, G.-Y., and J. Slingo, 2001: The diurnal cycle in the tropics. *Mon. Wea. Rev.*, **129**, 784–801, doi:10.1175/1520-0493(2001)129<0784:TDCITT>2.0.CO;2.

Yasunari, T., 1979: Cloudiness fluctuations associated with the Northern Hemisphere summer monsoon. *J. Meteor. Soc. Japan*, **57**, 227–242.

Zhang, C., 2005: Madden–Julian oscillation. *Rev. Geophys.*, **43**, RG2003, doi:10.1029/2004RG000158.

——, 2013: Madden–Julian oscillation: Bridging weather and climate. *Bull. Amer. Meteor. Soc.*, **94**, 1849–1872, doi:10.1175/BAMS-D-12-00026.1.